

Supplementary Part

**Turning on the red phosphorescence of a [Ru(tpy)(bpy)(Cl)]Cl complex by  
amide substitution: self-aggregation, toxicity, and localization of an  
emissive ruthenium-based amphiphile**

B. Siewert, M. Langerman, Y. Hontani, J.T.M. Kennis, V.H.S. van Rixel, B. Limburg, M.A. Siegler, V. Saez-Talens,  
R.E. Kieltyka, S. Bonnet\*

**Contents**

1. Material & Methods.....	2
1.1. General.....	2
1.2. Overview of all discussed structures.....	3
1.3. Synthesis .....	4
1.3.1. Synthesis of N-dodecyl-[2,2':6',2''-terpyridine]-4'-carboxamide ( <b>5</b> ).....	4
1.3.2. Synthesis of [Ru( <b>5</b> )(bpy)(Cl)]Cl – ([ <b>4</b> ]Cl) .....	5
1.3.3. [Ru( <b>5</b> )(bpy)(H <sub>2</sub> O)](NO <sub>3</sub> ) <sub>2</sub> (compound [ <b>7</b> ](NO <sub>3</sub> ) <sub>2</sub> ) .....	7
1.4. Single Crystal X-ray Crystallography.....	8
1.4.1. Crystal growing .....	8
1.4.2. Crystal structure determination .....	8
1.4.1. Crystal structure determination .....	8
1.4.2. Picture of the triclinic cell .....	10
1.4.3. Comparison of the distortion .....	10
2. Photophysical and Photochemical Studies.....	11
2.1. Determination of extinction coefficients .....	11
2.2. Emission Spectroscopy.....	12
2.2.1. Emission vs concentration in Water .....	12
2.2.2. Emission in several solvents .....	13
2.3. Life-time Measurements.....	14
2.3.1. Stability Studies .....	14
2.3.2. Transient absorption spectroscopy: .....	15
2.3.3. Time-correlated single photon counting (TCSPC):.....	16
2.3.4. Overview of the Results Life-Times .....	16
2.4. Photochemical Investigations .....	18
2.4.1. General Experimental Setup.....	18
2.4.2. Evolution of the UV-vis spectrum of [ <b>4</b> ]Cl in the dark and under light irradiation .....	18

2.4.3.	Calculation of the photosubstitution quantum yield for [4]Cl in water .....	20
3.	Self-Assembly of [4] <sup>+</sup> .....	23
3.1.	Calculation of the Molecular Packing Parameter.....	23
3.1.1.	General Formula .....	23
3.1.2.	Deriving Molecule Specific Values for [4] <sup>+</sup> .....	23
3.1.3.	Calculation of P .....	23
3.2.	Dynamic light scattering (DLS) and zeta-potential measurements.....	24
3.2	Cryo-Transmission electron microscopy (cryo-TEM).....	25
4.	Biological Studies.....	26
4.1.	Cell Culturing.....	26
4.2.	Cytotoxicity Studies.....	26
4.3.	Microscopic Uptake Studies.....	27
5.	DFT calculations .....	29
6.	Literature.....	29

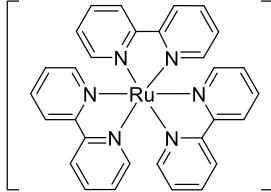
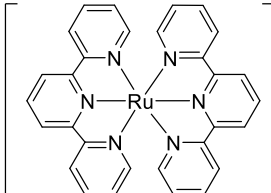
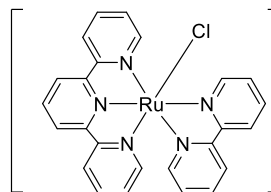
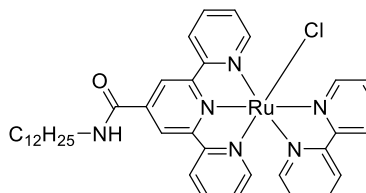
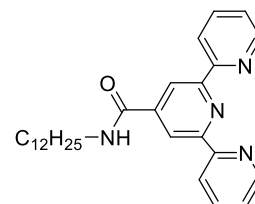
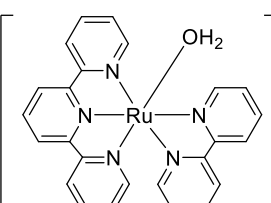
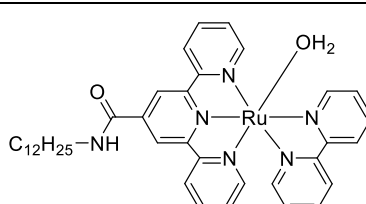
## 1. Material & Methods

### 1.1. General

<sup>1</sup>H NMR spectra were recorded using a Bruker DPX-300 spectrometer; chemical shifts are indicated in ppm relative to TMS. Electrospray mass spectra were recorded on a Finnigan TSQ-quantum instrument by using an electrospray ionization technique (ESI-MS). UV-Vis spectra were obtained on a Varian Cary 50 UV-visible spectrometer. The Dynamic Light Scattering (DLS) was performed with a Zetasizer instrument operating at  $\lambda_{\text{irr}} = 632$  nm from Malvern. The irradiation setup for UV-vis experiments consisted of custom made LEDs directly placed on top of a 1 cm quartz cuvet, as described by Bahreman *et al.*<sup>[1]</sup> Confocal pictures were obtained with a Leica TCS SPE system. Images and data were processed with Origin Pro, MetsreNova, ImageJ, ChemDraw, Gimp 2.0, and Microsoft Excel software.

## 1.2. Overview of all discussed structures

Table S 1. Overview of all structures discussed in the communication and in the supplementary part.

#	Formula	Structure	Synthesis
[1] <sup>2+</sup>	[Ru(bpy) <sub>3</sub> ] <sup>2+</sup>	 The structure shows a central Ruthenium (Ru) atom coordinated to three bipyridine (bpy) ligands in an octahedral geometry. The entire complex is enclosed in square brackets with a 2+ charge indicated at the top right.	-
[2] <sup>2+</sup>	[Ru(tpy) <sub>2</sub> ] <sup>2+</sup>	 The structure shows a central Ruthenium (Ru) atom coordinated to two terpyridine (tpy) ligands in an octahedral geometry. The entire complex is enclosed in square brackets with a 2+ charge indicated at the top right.	-
[3] <sup>+</sup>	[Ru(tpy)(bpy)Cl] <sup>+</sup>	 The structure shows a central Ruthenium (Ru) atom coordinated to one terpyridine (tpy) ligand, one bipyridine (bpy) ligand, and one chloride (Cl) ligand. The entire complex is enclosed in square brackets with a + charge indicated at the top right.	-
[4] <sup>+</sup>	[Ru(Rtpy)(bpy)Cl] <sup>+</sup>	 The structure shows a central Ruthenium (Ru) atom coordinated to one Rtpy ligand, one bipyridine (bpy) ligand, and one chloride (Cl) ligand. The Rtpy ligand has a dodecyl chain (C <sub>12</sub> H <sub>25</sub> -NH) attached to its 4' position. The entire complex is enclosed in square brackets with a + charge indicated at the top right.	S5
5	Rtpy=N-dodecyl-[2,2':6',2''-terpyridine]-4'-carboxamide	 The structure shows the Rtpy ligand, which is N-dodecyl-[2,2':6',2''-terpyridine]-4'-carboxamide. It consists of a terpyridine core with a dodecyl chain (C <sub>12</sub> H <sub>25</sub> -NH) attached to the 4' position of the central ring.	S4
[6] <sup>2+</sup>	[Ru(tpy)(bpy)(OH <sub>2</sub> )] <sup>2+</sup>	 The structure shows a central Ruthenium (Ru) atom coordinated to one terpyridine (tpy) ligand, one bipyridine (bpy) ligand, and one water (OH <sub>2</sub> ) ligand. The entire complex is enclosed in square brackets with a 2+ charge indicated at the top right.	-
[7] <sup>2+</sup>	[Ru(Rtpy)(bpy)(OH <sub>2</sub> )] <sup>2+</sup>	 The structure shows a central Ruthenium (Ru) atom coordinated to one Rtpy ligand, one bipyridine (bpy) ligand, and one water (OH <sub>2</sub> ) ligand. The Rtpy ligand has a dodecyl chain (C <sub>12</sub> H <sub>25</sub> -NH) attached to its 4' position. The entire complex is enclosed in square brackets with a 2+ charge indicated at the top right.	S6

### 1.3. Synthesis

Lithium chloride (LiCl), and triethylamine (NEt<sub>3</sub>) were purchased from Sigma-Aldrich, silver hexafluorophosphate (AgPF<sub>6</sub>) and 2,2':6',2''-terpyridine-4'-carboxylic acid from Acros Organics, and 2,2'-bipyridine (bpy) from Brunschwig Chemie. All reactants and solvents were used without further purification. The synthesis scheme for complex [4]Cl is given in Figure S 1.

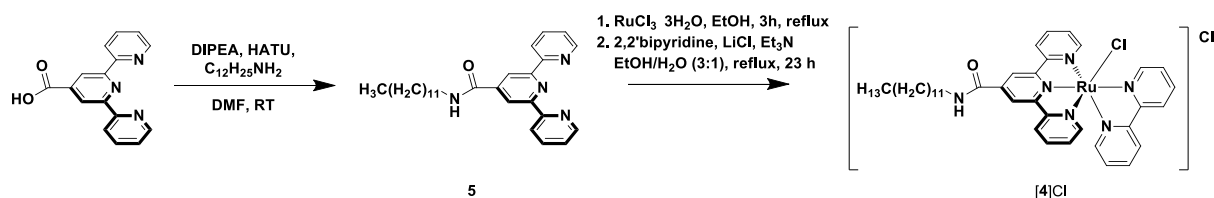


Figure S 1: Synthesis scheme for compound [4]Cl.

#### 1.3.1. Synthesis of N-dodecyl-[2,2':6',2''-terpyridine]-4'-carboxamide (5)

To a solution of 2,2':6',2''-terpyridine-4'-carboxylic acid (1.00 g, 3.60 mmol) in DMF (30 mL) was added HATU (1.50 g, 3.96 mmol), followed by DIPEA (1.30 mL, 7.92 mmol). After five minutes stirring, dodecyl amine (730 mg, 4.0 mmol) was added to the brown solution. The reaction mixture was stirred for an additional hour, poured into DCM, and washed with saturated NaHCO<sub>3</sub> solution (2x 50 mL) and H<sub>2</sub>SO<sub>4</sub> solution (0.5 M, 2x 50 mL). The combined organic phases were dried over MgSO<sub>4</sub>, and the solvents were removed under vacuum to yield the crude product as a brown paste. Further purification by column chromatography on neutral alumina using a gradient of MeOH in DCM (100% DCM → 98:2 MeOH/DCM, Al<sub>2</sub>O<sub>3</sub>) afforded compound 5 (R<sub>f</sub> = 0.5 (DCM/MeOH 99:1) as a white powder (480 mg, 30 % yield). The numbering scheme for <sup>1</sup>H NMR interpretation and the NMR are depicted in Figure S 2.

<sup>1</sup>H NMR (300 MHz, CDCl<sub>3</sub>) δ 8.75 (s, 2H, 3'), 8.72 (ddd, <sup>3</sup>J = 4.8, <sup>4</sup>J = 1.6, <sup>5</sup>J = 0.8 Hz, 2H, 6), 8.61 (brd, J = 8.0 Hz, 2H, 3), 7.88 (ddd, <sup>3</sup>J = 7.8, 7.8, <sup>4</sup>J = 1.8 Hz, 2H, 4), 7.36 (ddd, <sup>3</sup>J = 7.5, 4.8, <sup>4</sup>J = 1.2 Hz, 2H, 5), 6.49 (t, <sup>3</sup>J = 5.6 Hz, NH), 3.51 (td, <sup>3</sup>J = 7.1, 6.2 Hz, 2H, α), 1.64 (tt, <sup>3</sup>J = 7.7, 7.7 Hz, 2H, β), 1.50 – 1.19 (m, 18H tail), 0.87 – 0.85 (t, <sup>3</sup>J = 6.6 Hz, 3H, ε) ppm; <sup>13</sup>C NMR (75 MHz, CDCl<sub>3</sub>) δ 165.9 (Cq, a), 156.6 (Cq, 2'), 155.6 (Cq, 1), 149.4 (CH, 5), 144.5 (Cq, 4'), 137.1 (CH, 3), 124.3 (CH, 4), 121.5 (CH, 2), 118.4 (CH, 3'), 40.5 (CH<sub>2</sub>, α), 32.1 (CH<sub>2</sub>, β), 29.8 (CH<sub>2</sub>, δ), 29.7 (CH<sub>2</sub>, δ), 29.5 (CH<sub>2</sub>, δ), 22.8 (δ), 14.3 (CH<sub>3</sub>, ε) ppm; FT-IR (cm<sup>-1</sup>) ν = 3284w, 2916s, 2848m, 1641m, 1587w, 1556m, 1554brs, 1478w, 1467s, 1457w, 1452w, 1437w, 1394m, 1371w, 1361w, 1352w, 1292w, 1285w, 1266w, 1114w, 1087w, 1071w, 1042w, 990w, 889w, 798s, 773w, 747w, 740s, 732s, 722s, 671s, 658s, 621m, 618w; HR/MS: m/z (calc. for C<sub>28</sub>H<sub>36</sub>N<sub>3</sub>O+H<sup>+</sup> = 445.2962 Da): found = 445.2958 Da [M+H]<sup>+</sup>.

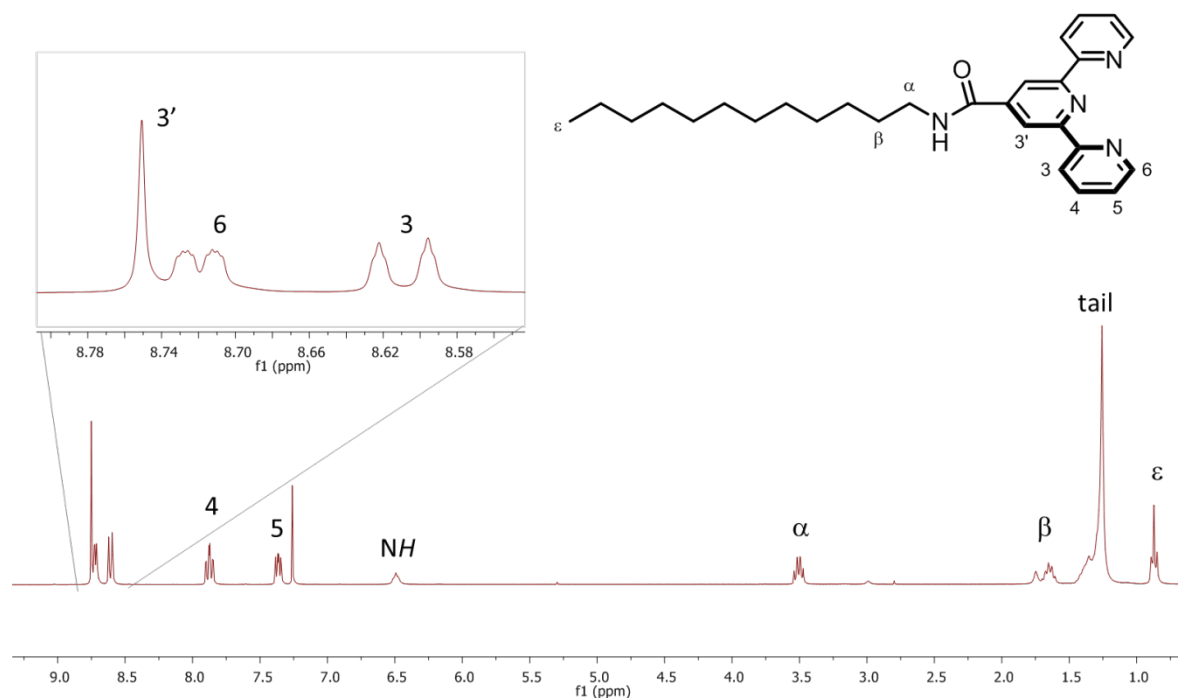


Figure S 2.  $^1\text{H-NMR}$  (300 MHz) of **5** in  $\text{CDCl}_3$  with assignment.

### 1.3.2. Synthesis of $[\text{Ru}(\mathbf{5})(\text{bpy})(\text{Cl})]\text{Cl} - ([\mathbf{4}]\text{Cl})$

Ruthenium(III) chloride trihydrate (167 mg, 0.4 mmol) was dissolved in ethanol (99.8%, 30 mL) and ligand **5** (178 mg, 0.4 mmol) was added. The mixture was stirred under reflux for four hours. After cooling down to RT the solid was filtered off, and washed with ethanol (150 mL) and diethylether (150 mL). The precursor  $[\text{Ru}(\mathbf{5})\text{Cl}_3]$  was obtained as a brown solid (260 mg, quantitative) and used without further purifications. In a second step,  $[\text{Ru}(\mathbf{5})\text{Cl}_3]$  (274 mg, 0.4 mmol) was dissolved with 2,2'-bipyridine (66 mg, 0.4 mmol) and LiCl (17.8 mg, 0.4 mmol) in a deoxygenated EtOH/ $\text{H}_2\text{O}$  (3:1) solution (40 mL), followed by the addition of  $\text{Et}_3\text{N}$  (90  $\mu\text{L}$ , 0.7 mmol). The resulting solution was stirred and refluxed for 18 hours under argon. The solvent was removed by rotary evaporation and the crude product was purified by silica column chromatography, using acetone/ $\text{H}_2\text{O}$ /1 M HCl (100:10:1) as the eluent. The fractions containing the product ( $R_f = 0.50$ ) were collected and the solvent removed by rotary evaporation. The crude product was further purified by alumina column chromatography, using DCM/MeOH (95:5) as the eluent. Following evaporation of the solvent, the product was precipitated from DCM in  $\text{Et}_2\text{O}$ , filtered off, and dried under vacuum, resulting in a dark purple solid. Yield: 305 mg (94%). The numbering scheme for  $^1\text{H}$  NMR interpretation is depicted in Figure S 3.

$^1\text{H}$  NMR (300 MHz,  $\text{DMSO-}d_6$ )  $\delta$  (ppm): 10.09 (d,  $^3J = 4.9$  Hz, 1H, A6), 9.23 (t,  $^3J = 5.8$  Hz, 1H, NH), 9.20 (s, 2H, T3'), 8.94 (d,  $^3J = 8.2$  Hz, 1H, A3), 8.78 (d,  $^3J = 8.0$  Hz, 2H, T3), 8.65 (d,  $^3J = 8.1$  Hz, 1H, B3), 8.39 (ddd,  $^3J = 7.8$ , 7.8 Hz,  $^4J = 1.6$  Hz, 1H, A4), 8.09 (ddd,  $^3J = 7.4$ , 5.7 Hz,  $^4J = 1.2$  Hz, 1H, A5), 8.03 (ddd,  $^3J = 7.9$ , 7.9 Hz,  $^4J = 1.5$  Hz, 2H, T4), 7.83 – 7.74 (ddd,  $^3J = 8.1$ , 7.7 Hz,  $^4J = 1.3$  Hz, 1H, B4), 7.64 (dd,  $^3J = 5.6$  Hz,  $^4J = 1.4$  Hz, 2H, T6), 7.42 (ddd,  $^3J = 7.1$ , 5.5 Hz,  $^4J = 1.3$  Hz, 2H, T5), 7.33 (dd,  $^3J = 5.8$  Hz,  $^4J = 1.3$  Hz, 1H, B6), 7.05 (ddd,  $^3J = 7.3$ , 5.7 Hz,  $^4J = 1.3$  Hz, 1H, B5), 3.46 (dt,  $^3J = 6.7$ , 6.5 Hz, 2H, H $_{\alpha}$ ), 1.67 (tt,  $^3J = 7.1$ , 6.7 Hz, 2H, H $_{\beta}$ ), 1.49 – 1.13 (m, 16H, H $_{\gamma}$ +H $_{\delta}$ ), 0.84 (t,  $^3J = 6.6$  Hz, 3H, H $_{\epsilon}$ );  $^{13}\text{C}$  NMR (75 MHz,  $\text{DMSO-}$

$d_6$ )  $\delta$  (ppm): 163.6 (C=O), 158.1 (T2'), 158.1 (A2), 157.8 (T2), 155.4 (B2), 151.9 (A6), 151.8 (T6), 151.7 (B6), 138.6 (T4'), 137.3 (T4), 137.0 (A4), 135.9 (B4), 127.7 (T5), 127.1 (A5), 126.5 (B5), 124.0 (T3), 123.8 (A3), 123.6 (B3), 120.4 (T3'), 39.7 (C $_{\alpha}$ ), 31.3 (C $_{\delta}$ ), 29.1 (C $_{\delta}$ ), 28.9 (C $_{\beta}$ ), 28.8 (C $_{\delta}$ ), 26.6 (C $_{\gamma}$ ), 22.1 (C $_{\delta}$ ), 14.0 (C $_{\epsilon}$ ); IR  $\nu$  (cm $^{-1}$ ) = 2926m, 2850m, 1612w, 1601w, 1465m, 1442w, 1419m, 1394m, 1252m, 1226s, 1215s, 1161m, 1157m, 1061w, 1015s, 792w, 772m, 760m, 730brs, 696w, 660m, 655w, 609m; Elemental analysis calcd (%) for C $_{38}$ H $_{44}$ Cl $_2$ N $_6$ ORu + 0.5 H $_2$ O: C 58.38, H 5.80, N 10.75; found: C 58.13, H 5.51, N 10.59; UV-Vis:  $\lambda_{\text{max, MLCT}}$  ( $\epsilon$  in L mol $^{-1}$  cm $^{-1}$ ) in MeOH = 235 (19469), 285 (25304), 325 (16683), 505 (6759) nm; ESI MS  $m/z$  (calc): 737.2 (737.2, [M-Cl] $^+$ ).

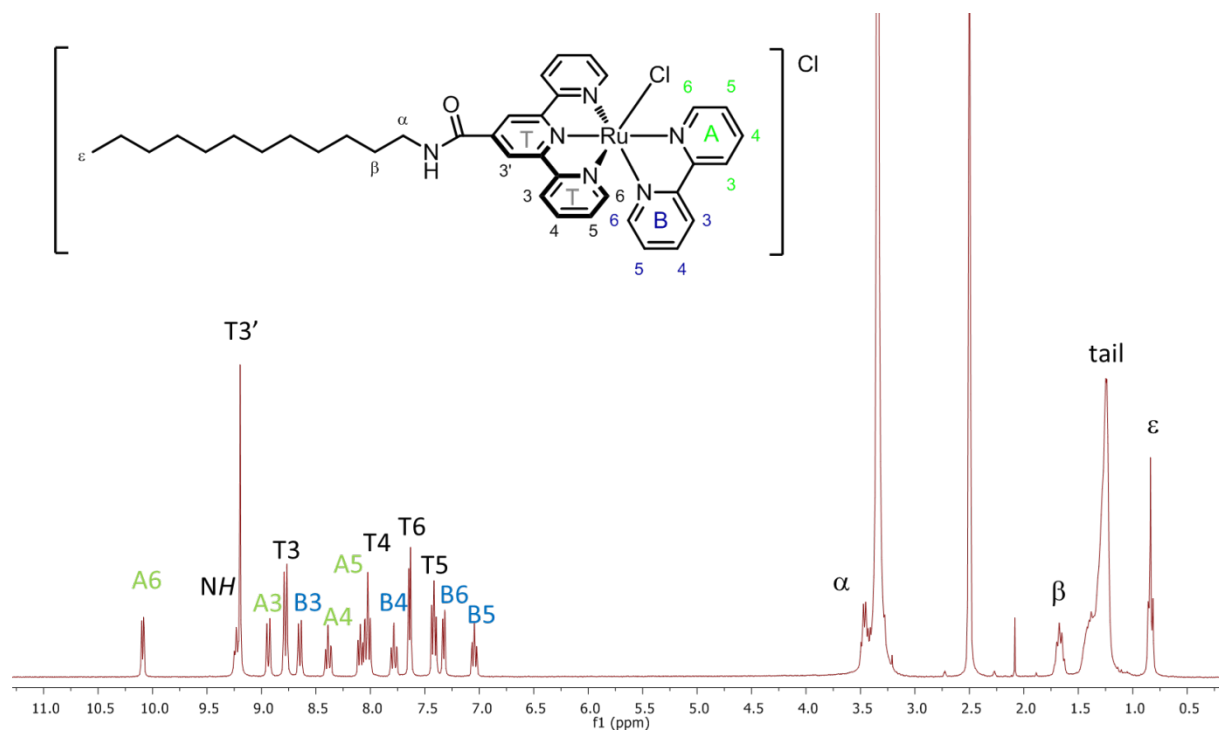
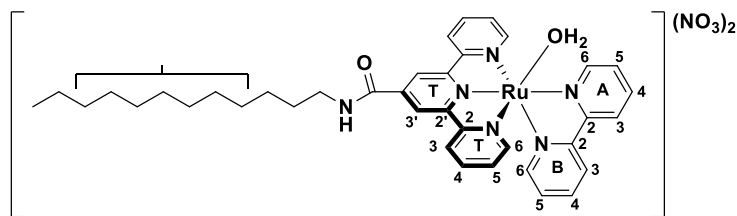


Figure S 3.  $^1\text{H-NMR}$  of [4]Cl in  $d_6$ -DMSO with assignment.

1.3.3. [Ru(5)(bpy)(H<sub>2</sub>O)](NO<sub>3</sub>)<sub>2</sub> (compound [7](NO<sub>3</sub>)<sub>2</sub>)



Complex [4]Cl (20 mg, 26  $\mu$ mol) and AgNO<sub>3</sub> (11 mg, 65  $\mu$ mol) were dissolved in a deoxygenated H<sub>2</sub>O/Aceton (3:1) solution (16 mL). The resulting solution was refluxed for 24 hours under argon. The

solution was then filtered over a glass filter to remove AgCl, and the solvents were evaporated by rotary evaporation. The crude product was loaded on an alumina column using acetone/H<sub>2</sub>O (95:5  $\rightarrow$  100:10) as the eluent ( $R_f$  = 0.25). After evaporation of the solvents by rotary evaporation at 303 K, alumina TLC (acetone/H<sub>2</sub>O [95:5]) showed two spots (the nitro and aqua complexes at  $R_f$  = 0.66 and 0.25, respectively), but <sup>1</sup>H NMR measurement in D<sub>2</sub>O showed the presence of a single complex. Yield: 17 mg (78%). <sup>1</sup>H NMR (400 MHz, D<sub>2</sub>O)  $\delta$  9.53 (d, <sup>3</sup> $J$  = 5.6 Hz, 1H, A6), 8.86 (s, 2H, T3'), 8.69 (d, <sup>3</sup> $J$  = 8.3 Hz, 1H, A3), 8.52 (d, <sup>3</sup> $J$  = 8.1 Hz, 2H, T3), 8.35 (m, 2H, A4+B3), 8.02 (m, 3H, A5+T4), 7.81 (d, <sup>3</sup> $J$  = 5.8 Hz, 2H, T6), 7.68 (dd, <sup>3</sup> $J$  = 8.0, 8.0 Hz, 1H, B4), 7.37 (m, 2H, T5), 7.19 (d, <sup>3</sup> $J$  = 5.8 Hz, 1H, B6), 6.93 (m, 1H, B5), 3.59 (t, <sup>3</sup> $J$  = 6.6 Hz, 2H, H <sub>$\alpha$</sub> ), 1.76 (m, 2H, H <sub>$\beta$</sub> ), 1.53 – 1.45 (m, 2H, H <sub>$\gamma$</sub> ), 1.02 (m, 14H, H <sub>$\delta$</sub> ), 0.88 (m, 2H, H <sub>$\phi$</sub> ), 0.86 – 0.77 (m, 2H, H <sub>$\delta$</sub> ), 0.55 (t, <sup>3</sup> $J$  = 7.2 Hz, 3H, H <sub>$\epsilon$</sub> ) ppm; UV-Vis:  $\lambda_{max}$  ( $\epsilon$  in L mol<sup>-1</sup> cm<sup>-1</sup>) in pure H<sub>2</sub>O: 204 (46.1 $\times$ 10<sup>3</sup>), 283 (26.2 $\times$ 10<sup>3</sup>), 322 (18.1 $\times$ 10<sup>3</sup>), 492 nm (6.0 $\times$ 10<sup>3</sup>).

## 1.4. Single Crystal X-ray Crystallography

### 1.4.1. Crystal growing

Single crystals of [4]Cl were obtained by crystallization via liquid-vapor diffusion using acetone as solvent and diisopropyl ether as counter-solvent. In short, [4]Cl (1.2 mg) was dissolved in acetone (2 mL), and placed in a MS vial. This vial was placed in a larger vial containing diisopropyl ether (2.8 mL). The large vial was closed and vapor diffusion occurred within a few days to afford X-ray quality single crystals.

### 1.4.2. Crystal structure determination

All reflection intensities were measured at 110(2) K using a SuperNova diffractometer (equipped with Atlas detector) with Cu  $K\alpha$  radiation ( $\lambda = 1.54178 \text{ \AA}$ ) under the program CrysAlisPro (Version 1.171.36.32 Agilent Technologies, 2013). The same program was used to refine the cell dimensions and for data reduction. The structure was solved with the program SHELXS-2014/7 (Sheldrick, 2015) and was refined on  $F^2$  with SHELXL-2014/7 (Sheldrick, 2015). Analytical numeric absorption correction using a multifaceted crystal model was applied using CrysAlisPro. The temperature of the data collection was controlled using the system Cryojet (manufactured by Oxford Instruments). The H atoms were placed at calculated positions using the instructions AFIX 23, AFIX 43 or AFIX 137 with isotropic displacement parameters having values 1.2 or 1.5  $U_{eq}$  of the attached C or N atoms. The H atoms attached to O1W/O1W' could not be retrieved reliably from difference Fourier maps due to disorder. The structure is partly disordered. The experimental details are given in Table S 2

#### Additional notes:

The counterion  $\text{Cl}^-$  (Cl2) and the lattice water molecule (O1W) are both disordered over two orientations. The occupancy factors of the major components of the disorder refine to 0.820(5) and 0.515(16), respectively.

### 1.4.1. Crystal structure determination

Table S 2. Crystal structure data for [4]Cl · H<sub>2</sub>O · CH<sub>3</sub>COCH<sub>3</sub>.

Chemical formula	C <sub>38</sub> H <sub>44</sub> ClN <sub>6</sub> ORu·C <sub>3</sub> H <sub>6</sub> O·Cl·O
$M_r$	846.84
Crystal system, space group	Triclinic, $P-1$
Temperature (K)	110
$a, b, c$ (Å)	8.7702 (4), 14.3952 (9), 16.7553 (6)
$\alpha, \beta, \gamma$ (°)	100.353 (4), 99.430 (3), 99.857 (4)
$V$ (Å <sup>3</sup> )	2008.42 (18)
$Z$	2
Radiation type	Cu $K\alpha$
$\mu$ (mm <sup>-1</sup> )	4.75
Crystal size (mm)	0.20 × 0.09 × 0.01

Data collection	
Diffractometer	SuperNova, Dual, Cu at zero, Atlas diffractometer
Absorption correction	Analytical <i>CrysAlis PRO</i> , Agilent Technologies, Version 1.171.36.32 (release 02-08-2013 CrysAlis171 .NET) (compiled Aug 2 2013,16:46:58) Analytical numeric absorption correction using a multifaceted crystal model based on expressions derived by R.C. Clark & J.S. Reid. (Clark, R. C. & Reid, J. S. (1995). <i>Acta Cryst.</i> A51, 887-897)
$T_{\min}, T_{\max}$	0.485, 0.939
No. of measured, independent and observed [ $I > 2\sigma(I)$ ] reflections	17876, 7212, 6053
$R_{\text{int}}$	0.042
$(\sin \theta/\lambda)_{\text{max}}$ ( $\text{\AA}^{-1}$ )	0.598
Refinement	
$R[F^2 > 2\sigma(F^2)], wR(F^2), S$	0.041, 0.105, 1.03
No. of reflections	7212
No. of parameters	501
No. of restraints	12
H-atom treatment	H-atom parameters constrained
$\Delta\rho_{\text{max}}, \Delta\rho_{\text{min}}$ ( $\text{e \AA}^{-3}$ )	0.95, -0.92

Computer programs: *CrysAlis PRO*, Agilent Technologies, Version 1.171.36.32 (release 02-08-2013 CrysAlis171 .NET) (compiled Aug 2 2013, 16:46:58), *SHELXS2014/7* (Sheldrick, 2015), *SHELXL2014/7* (Sheldrick, 2015), *SHELXTL* v6.10 (Sheldrick, 2008)<sup>[2]</sup>.

### 1.4.2. Picture of the triclinic cell

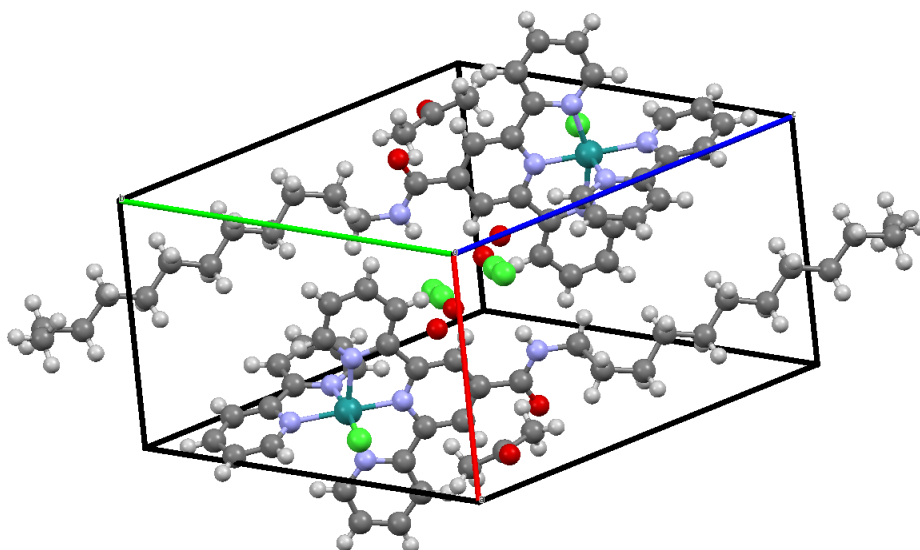


Figure S 4. Packing of [4]Cl in the triclinic cell. The two complexes are related to each other by inversion symmetry.

### 1.4.3. Comparison of the distortion

Data for [3](PF<sub>6</sub>)<sub>2</sub> was obtained from the Cambridge Crystallographic Data Centre (CCDC, 789502), and the distances as well as the angles (see Table S 3) extracted with Mercury. A side view of the crystal structure of the parental complex [3]<sup>+</sup> is given for comparison with [4]<sup>+</sup> in Figure S 5. The crystal data of [4]Cl was submitted to the Cambridge Crystallographic Data Centre, and got the following deposition number: CCDC 1534260.

Table S 3: Compilation of structural data obtained for [4]Cl, with data for [3]Cl available from the CCDC database.

	[3](PF <sub>6</sub> ) Distance [Å]	[4]Cl Distance [Å]
<b>Ru-N1</b>	2.069(2)	2.077(3)
<b>Ru-N2</b>	2.031(2)	2.049(3)
<b>Ru-N3</b>	2.059(2)	2.067(3)
<b>Ru-N4</b>	1.951(2)	1.954(3)
<b>Ru-N5</b>	2.070(2)	2.076(2)
<b>Ru-Cl</b>	2.3969(7)	2.3956(9)
	Angle [°]	Angle [°]
<b>N3-Ru-N5</b>	159.38(9)	159.4(1)

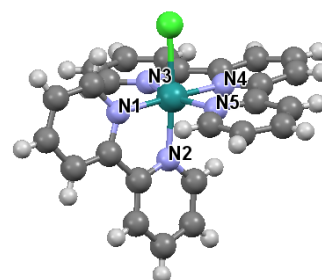


Figure S 5: Crystal structure of [3](PF<sub>6</sub>) with relevant atom labelling.

## 2. Photophysical and Photochemical Studies

### 2.1. Determination of extinction coefficients

Stock solutions of [4]Cl in MeOH were prepared. A series of five different concentrations was prepared ( $c = 65.6 \mu\text{M}$ ,  $54.6 \mu\text{M}$ ,  $45.5 \mu\text{M}$ ,  $37.9 \mu\text{M}$ ,  $31.6 \mu\text{M}$ ) and transferred to a quartz cuvette filled with 3 mL solution. Fast absorbance spectra were measured for each sample (Figure S 6) to determine the extinction coefficient from the slope of a plot of the absorbance vs. concentration at each wavelength with the set term  $f(0) = 0$ . The resulting curve was linear, showing that no self-assembly occurred in MeOH, which was confirmed by DLS measurements of a  $200 \mu\text{M}$  solution of [4]Cl in methanol.

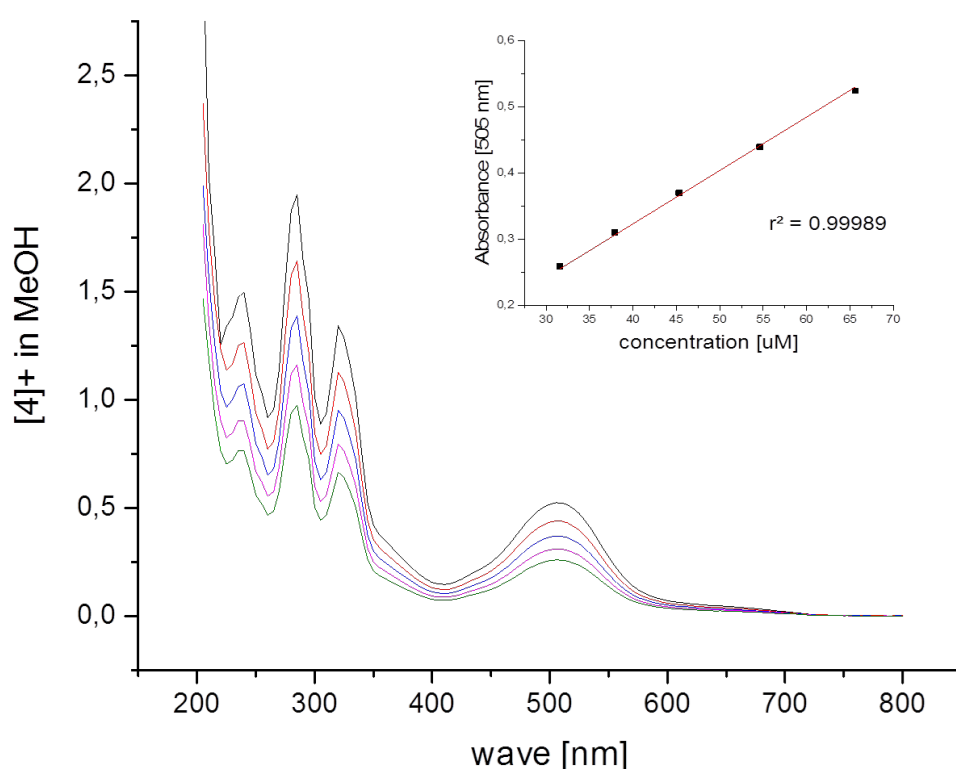
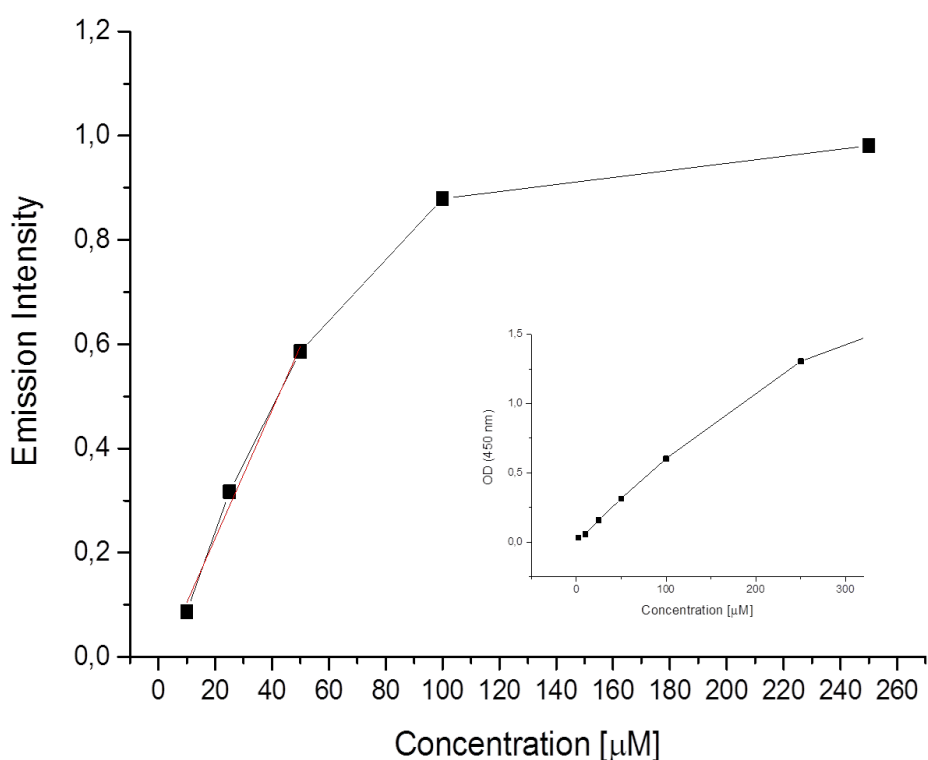


Figure S 6.: Electron absorption spectra of a concentration series of [4]Cl in methanol. Inlet shows the plot of the concentration vs absorbance at 505 nm, which was used to determine epsilon.

## 2.2. Emission Spectroscopy

### 2.2.1. Emission vs concentration in Water

A stock solutions of [4]Cl (500  $\mu\text{M}$  in MilliQ water) was prepared and diluted to 250, 100, 50, 25, 10, and 2.5  $\mu\text{M}$ . Emission spectra with the excitation wavelength of 450 nm (50 mW power) were measured on a Shimadzu RF 5301PC spectrofluorimeter at ambient atmosphere and under air, as described in Askes *et al.*<sup>[3]</sup> An absorbance spectra was measured before and after excitation to assure that no photochemical reaction had occurred, and that the spectrum was that of the chlorido complex [4]<sup>+</sup> (and not of the aqua complex [7]<sup>2+</sup>). Figure S7 shows the plotted emission intensity vs the concentration. In a concentration range below 60  $\mu\text{M}$  a linear correlation was observed ( $r^2 = 0.99$ ).



**Figure S7:** Emission intensity of [4]Cl vs concentration measured in MilliQ water; no appreciable hydrolysis occurred in the conditions of this experiment. The linear increase below 100  $\mu\text{M}$  indicates an absence of self-assembly and self-quenching effects. Inlet. Optical density at 450 nm for the several investigated concentrations of [4]Cl.

### 2.2.2. Emission in several solvents

The emission spectra of [4]Cl in DMF, acetone, ACN, MeOH, and pentane, were measured to rule out that the emission was induced by aggregation (Figure S8). In all solvents, including in water, emission spectra at an excitation wavelength of 450 nm (50 mW power) were measured on a Shimadzu RF 5301PC spectrofluorimeter at ambient atmosphere and under air, as described in Askes *et al.*<sup>[3]</sup> For MilliQ water an absorbance spectra was measured before and after measurement of the emission spectrum (typically after 15 min, Figure S8 bottom left), demonstrating that no (photochemical) hydrolysis reaction had occurred during emission measurement. Additional DLS measurement of [4]Cl in MeOH (data not shown) proved that the solution is free of any aggregation.

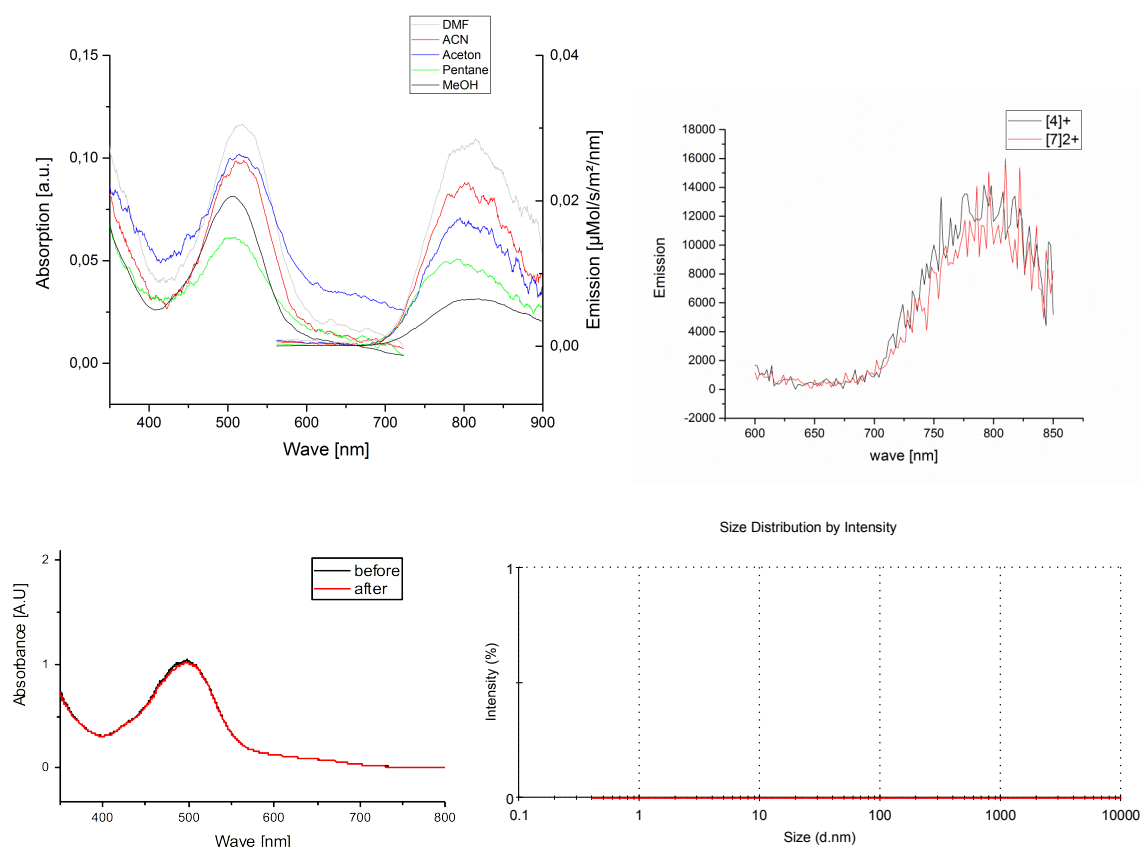


Figure S 8. Top left: UV-vis absorption and emission spectra of [4]Cl in different solvents, using an excitation wavelength of 450 nm. Top right: compared emission spectra of [4]Cl and [7](PF<sub>6</sub>)<sub>2</sub> in water. Bottom left: absorption spectrum of [4]Cl in MilliQ water before and after emission measurement; the superimposable spectra show aquation into [7]<sup>2+</sup> is negligible in such conditions. Bottom right: DLS of [4]Cl in MeOH showing the absence of self-assembly in this solvent.

## 2.3. Life-time Measurements

### 2.3.1. Stability Studies

Before starting the experiments, the stability of [4]Cl in presence or absence of chloride anions was investigated. Therefore electron absorptions spectra were measured every 20 min over a total period of 17 h. As shown in Figure S 9, [4]<sup>+</sup> was stable over a period of at least 17 h in PBS. Thus, the lifetime measurement in PBS only describe the excited states of [4]<sup>+</sup>. In PB (chloride-free buffer) the formation of [7]<sup>2+</sup> did take place within typically 4-6 h (see section 2.4. for more details).

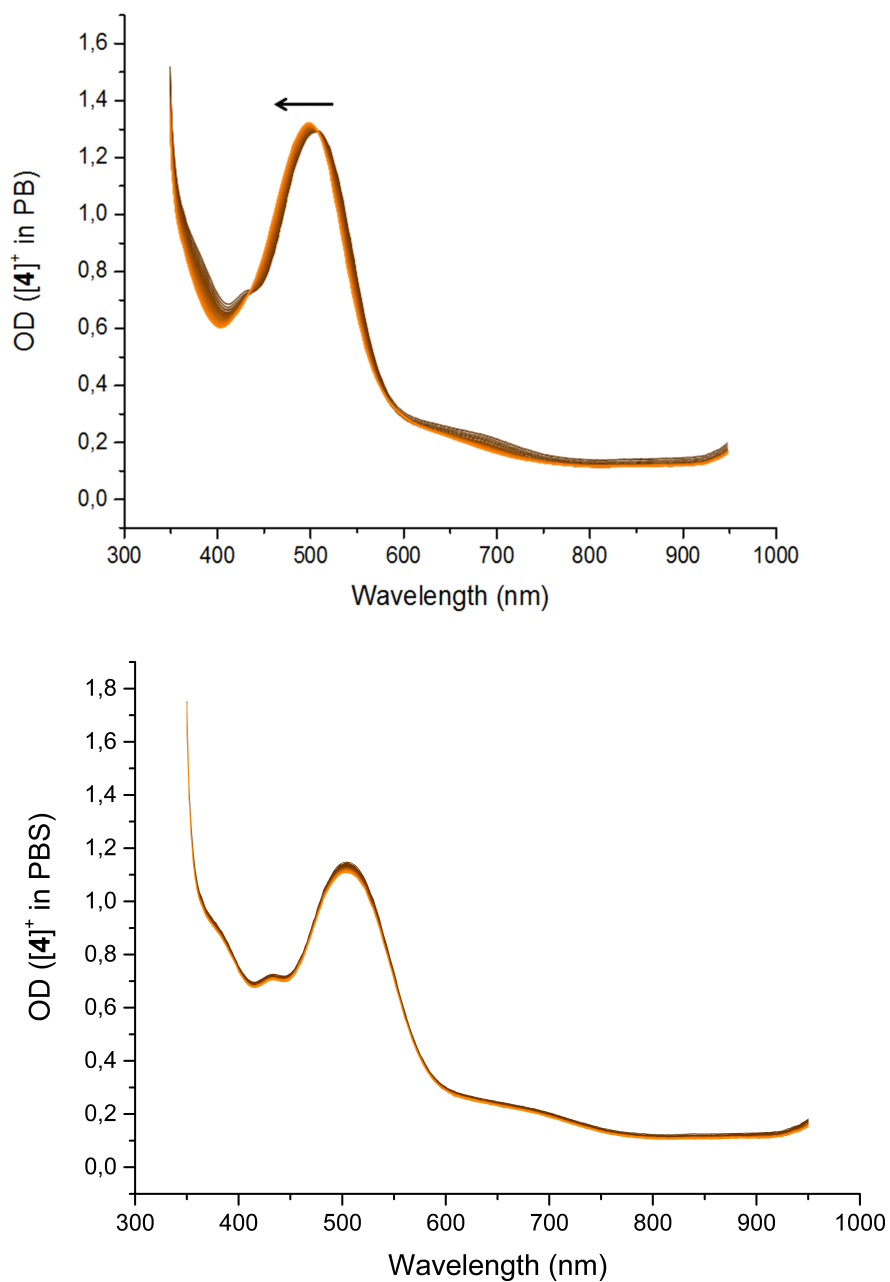


Figure S 9.: Stability of [4]<sup>+</sup> in aqueous solutions containing no chloride ions (PB, above) or with chloride ions (PBS, below).

### 2.3.2. Transient absorption spectroscopy:

Transient absorption measurements were performed with a femtosecond-to-microsecond pump-probe setup as reported previously<sup>[4]</sup> at room temperature ( $\sim 20^\circ\text{C}$ ). A sample of [4]Cl (75  $\mu\text{M}$ ) was dissolved in 10 mM phosphate-buffered saline (PBS) at pH 7.4 with  $\text{OD} \sim 4/\text{cm}$  at 500 nm, and filled in an 1-mm quartz cuvette (100-QS, Hellma Analytics) and set on a home-built vibrating sample holder in order to avoid damage to the samples. The wavelength of the pump beam was centered at 500 nm, and the laser power was attenuated to  $\sim 600$  nJ. A 2-mm thick  $\text{CaF}_2$  plate was used to generate white-light probe pulses, and a selected wavelength region at 370–670 nm was detected by the photodiode array. The time delays between the pump and probe pulses were varied up to 14  $\mu\text{s}$  at 103 data points with the minimum temporal step of 50 fs. The diameters of the pump and the probe beams at the sample position were  $\sim 200$   $\mu\text{m}$  and  $\sim 70$   $\mu\text{m}$ , respectively. Global analysis was performed for the transient absorption spectra using the Glotaran program.<sup>[4-5]</sup> With global analysis, all wavelengths were analyzed simultaneously with a set of common time constants<sup>[6]</sup>. A kinetic model was applied consisting of sequentially interconverting, evolution-associated difference spectra (EADS), *i.e.*  $1 \rightarrow 2 \rightarrow 3 \rightarrow \dots$  in which the arrows indicate successive mono-exponential decays of a time constant, which can be regarded as the lifetime of each EADS.<sup>[6]</sup> The first EADS corresponds to the difference spectrum at time zero. The first EADS evolves into the second EADS with time constant  $\tau_1$ , which in turn evolves into the third EADS with time constant  $\tau_2$ , etc. The procedure clearly visualizes the evolution of the intermediate states of the molecule<sup>[7]</sup>. Decay-associated difference spectra (DADS) indicate the spectral changes with parallel decay channels and independent decay time constants. It is important to note that the parallel and the sequential analysis are mathematically equivalent and yield identical time constants<sup>[8]</sup>. The standard errors in the time constants were less than 5%. The instrumental response function was  $\sim 50$  fs, estimated from the global analysis. Globally fitted transient absorption spectra (TAS) are shown in Fig. S10. Five components were required for adequate fitting: <50 fs, 2.8 ps, 110 ps, 17 ns and Infinite (Table S4). The positive signals show excited-state absorption (ESA), and the negative signals at 400–570 nm show ground-state bleach (GSB), which is caused by depletion of the ground-state species.

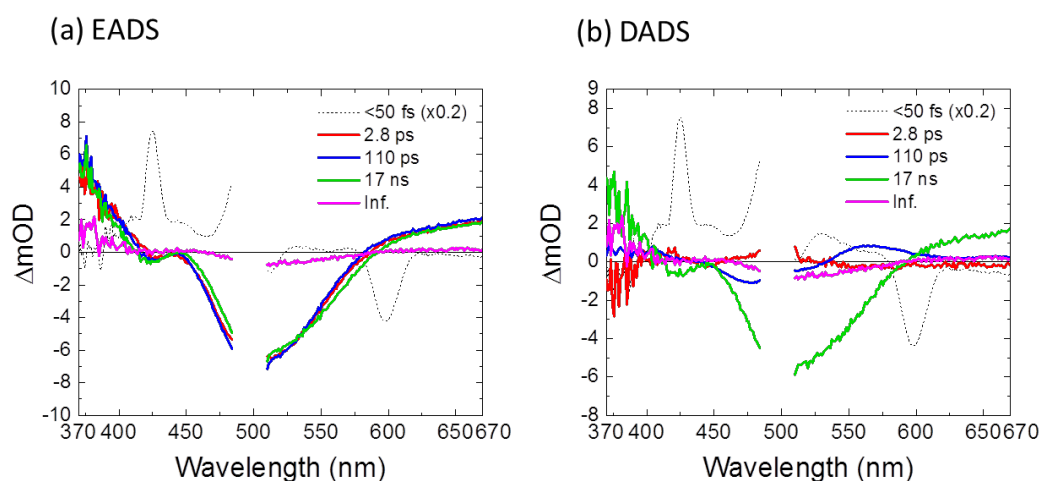


Figure S 10. a) Evolution-associated difference spectra (EDAS) of [4]Cl after global fitting. B) Decay-associated difference spectra (DADS). The wavelength region of 485–510 nm is omitted because of the strong pump light scattering.

### 2.3.3. Time-correlated single photon counting (TCSPC):

Time-resolved emission experiment for [4]Cl (75  $\mu$ M) up to 400 ns was performed by time-correlated single photon counting (TCSPC) using FluoTime200 (Picoquant) at room temperature ( $\sim 20^\circ\text{C}$ ). The [4]Cl sample was solved in 10 mM phosphate-buffered saline (PBS) at pH 7.4, and diluted to an OD of  $\sim 0.4/\text{cm}$  at 500 nm. The sample was filled in a 10-mm pathlength plastic cuvette (759150, Brand), and stirred during experiments with a magnetic stirrer. The sample was excited with a 2.5 MHz pulsed diode laser (wavelength: 470 nm, pulse duration:  $<70$  ps, LDH P-C-470, Picoquant); the excitation power was attenuated to  $\sim 25$   $\mu$ W with a neutral density filter and focused to  $\sim 50$   $\mu$ m at the sample position. The emission was detected at 760 nm with a channel time spacing of 16 ps. Data analysis was performed by fitting software FluoFit (Picoquant). The instrument response function was  $\sim 70$  ps. Three exponential components were required for the fitting: 0.44 ns (44%),

9.0 ns (14%) and 40 ns (42%) (Table S4).

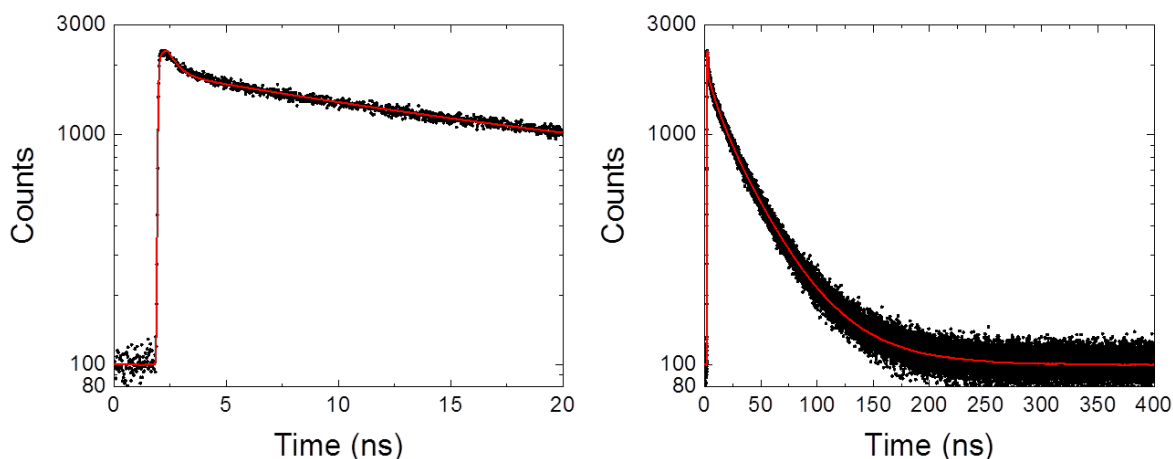


Figure S 11. Graph with fitting of the TCSPC experiment for [4]Cl in PBS. Left the zoom in (up to 20 ns) is shown, right the entire measured data.

### 2.3.4. Overview of the Results Life-Times

Interpretation of the observed lifetimes was done by the means of logical reasoning (e.g. blue-shift vs red shift of a lifetime, TCSPC and TAS), comparing the lifetimes to literature values, and to values found for similar complexes which lack the fatty tail (manuscript Siewert and Hontani *et al.* in preparation), thus effects of the supramolecular assembling can be excluded.

Table S 4 is a compilation of all lifetimes measured, which were obtained out of the two independent measurement types. Figure S 12 shows the lifetimes incorporated in a schematic Jablonski diagram. Excitation of tleads to population of the  $^1\text{MLCT}$  state, which decays quickly ( $\tau_1 < 50$  fs) to the  $^3\text{MLCT}$  state. The transient absorption spectra was slightly blue shifted ( $\tau_2 = 2.8$  ps), indicating vibrational relaxation on  $^3\text{MLCT}$  occurs in 2.8 ps.

Since the lifetime of  $^1\text{MLCT}$  is very short ( $<50$  fs) and the  $^3\text{MC}$  state are usually considered as non-radiative, it can be considered that all the emission components measured by TCSPC are from the  $^3\text{MLCT}$  state. Thus, the emission lifetimes directly reflect the lifetimes of the  $^3\text{MLCT}$  state. In 440

ps, a large part (44%) of the emission disappeared, indicating that the population of the  $^3\text{MLCT}$  state largely decreased in 440 ps. On the other hand, in TAS, only little recovery of the GSB was observed in 110 ps, which is probably from the same kinetic species as the 440-ps component in TCSPC. This observation shows that decay from the  $^3\text{MLCT}$  to the ground state barely happened in 110 ps. Thus, the 440-ps component in TCSPC (110 ps in TAS) is assigned to transition from  $^3\text{MLCT}$  to  $^3\text{MC}$ . In the nanosecond time region, two emission components were seen: 9.0 ns (14%) and 40 ns (42%), indicating that the population of the  $^3\text{MLCT}$  decayed with those two time constants. In addition, In TAS, the GSB mostly decayed in similar time range (17 ns), which means the ground state population recovered largely in 17 ns. These observations imply that ground-state recovery from the  $^3\text{MLCT}$  state occurred in 9.0 ns and 40 ns. In the final component in TAS (200 ns), slight recovery of the GSB was seen, while no emission component was observed in a similar time scale. Therefore, the 200-ns component can be assigned to the  $^3\text{MC}$  state decay to the ground state.

Table S 4: Overview of the obtained lifetimes for  $[4]^+$  in PBS.

	Absorption (TAS)	Emission (TCSPC, @760 nm)
$\tau_1$	< 50 fs	
$\tau_2$	2.8 ps	
$\tau_3$	110 ps	0.44 ns (44%)
$\tau_4$	17 ns	9.0 ns ( $\tau_{4a}$ , 14%) and 40 ns ( $\tau_{4b}$ , 42%)
$\tau_5$	200 ns	

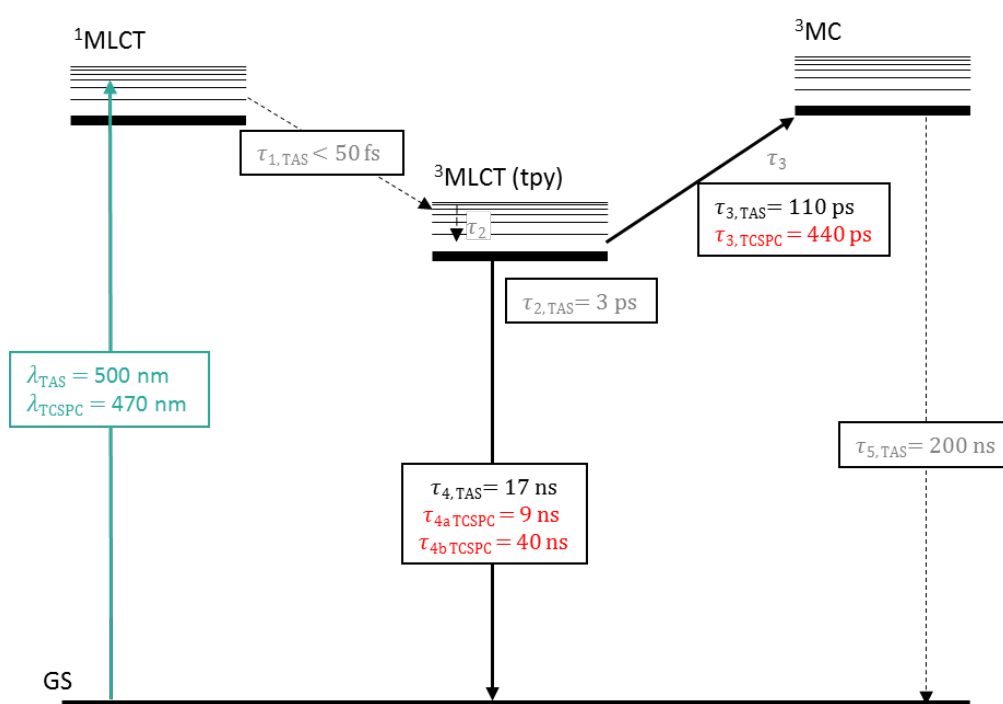


Figure S 12. Jablonski diagram for  $[4]\text{Cl}$  with lifetimes found in PBS. Red highlighted are the emissive lifetimes from the TCSPC experiment, black those from the TAS experiment.

## 2.4. Photochemical Investigations

### 2.4.1. General Experimental Setup

A stock solution of [4]Cl (0.47 mg in 5 mL milliQ Water,  $1.2 \times 10^{-4}$  M) was prepared. To investigate the photochemical properties of complex [4]Cl, 1 mL of the stock solution was added to a quartz cuvette filled with 2.00 mL H<sub>2</sub>O. The sample was deoxygenated with argon for 15 minutes. Irradiation was done using a custom 490 nm light emitting diode (LED) for 172 minutes, and the samples were stirred under argon and kept at 24 °C for the duration of the experiment. During irradiation UV-vis absorbance spectra were measured at variable time intervals, ranging from every 0.5 to 10 minutes.<sup>[1]</sup> The aqua complex [7](NO<sub>3</sub>)<sub>2</sub> was synthesized independently, as described in 1.3.3., and its molar absorption coefficient determined to determine its concentration during irradiation of [4]Cl.

### 2.4.2. Evolution of the UV-vis spectrum of [4]Cl in the dark and under light irradiation

The evolution of the electronic absorption spectra in the dark and under green light irradiation (490 nm,  $2.17 \text{ J} \cdot \text{cm}^{-2}$ ) is shown in Figure S 13. In both settings a hypsochromic shift was observed, indicating the formation of the aqua species [7]<sup>2+</sup>. In the dark at a concentration of 20.2 μM, the thermal hydrolysis reaction needed roughly 6 h for completion; under light irradiation at a concentration of 34.9 μM only 20 min were necessary to see full hydrolysis. Hydrolysis is thus accelerated by light irradiation.

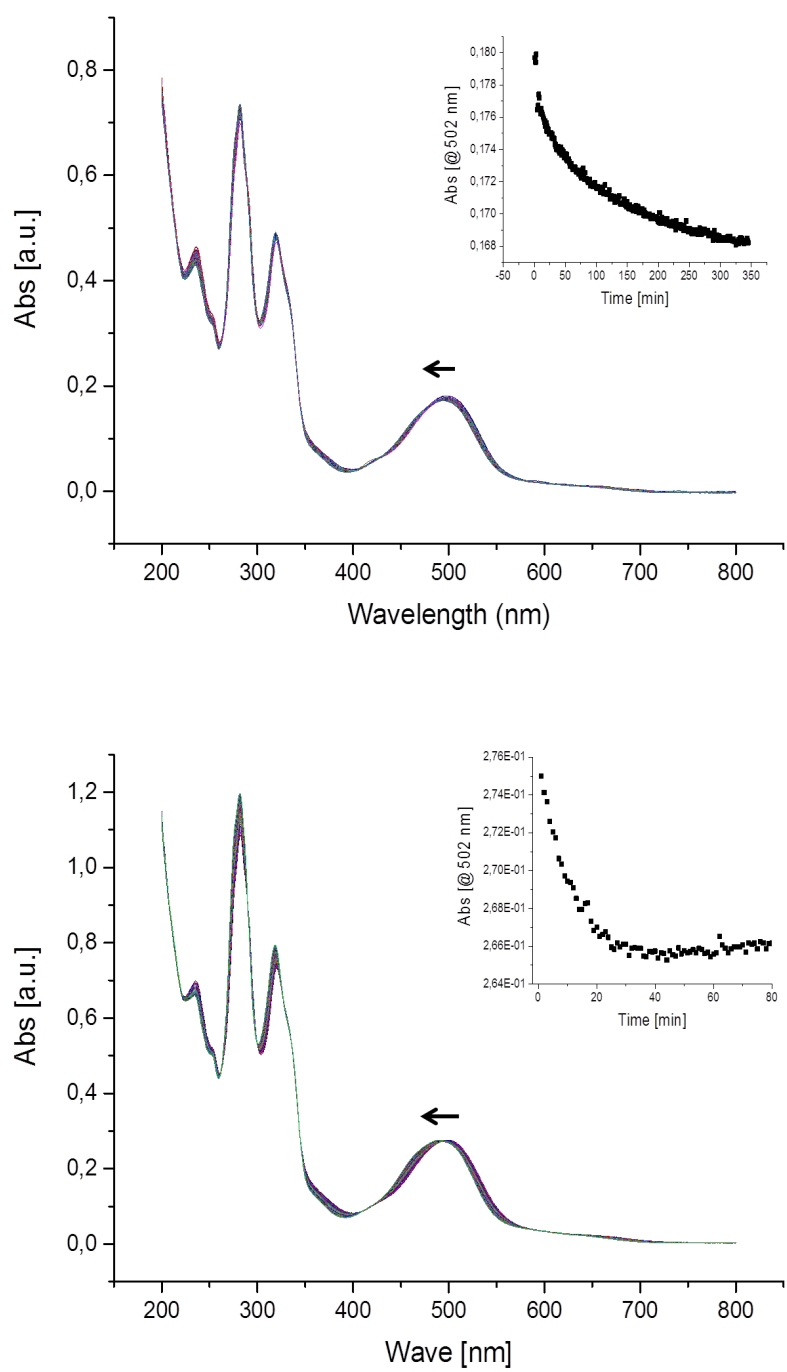


Figure S 13.: Evolution of the electron absorption spectrum of [4]Cl in MilliQ water. Above: The sample was kept in the dark. Below: the sample was irradiated with green light (490 nm, 2.17 J·cm<sup>-2</sup>) perpendicularly to the beam of the UV-vis spectrophotometer. Inlet in each graph depicts the devolution of the optical density at the absorption maxima of [4]<sup>+</sup> (502 nm in water).

### 2.4.3. Calculation of the photosubstitution quantum yield for [4]Cl in water

As the absorbance at any time point during the irradiation of [4]Cl in water is a combination of the absorption of both the ruthenium chloride species (hereafter noted RuCl) and the photosubstitution product (hereafter noted RuOH<sub>2</sub>), the concentration of RuCl was calculated according to a previously published protocol.<sup>[1]</sup> The absorbance at any wavelength can be described with Equation A1 and Equation A2.

$$A_{\lambda 1} = \varepsilon_{\lambda 1}^{RuS} \times l \times [RuCl] + \varepsilon_{\lambda 1}^{RuOH_2} \times l \times [RuOH_2] \quad (\text{Equation A1})$$

$$A_{\lambda 2} = \varepsilon_{\lambda 2}^{RuS} \times l \times [RuCl] + \varepsilon_{\lambda 2}^{RuOH_2} \times l \times [RuOH_2] \quad (\text{Equation A2})$$

Equation 1 can be rewritten as an expression of [RuOH<sub>2</sub>]:

$$[RuOH_2] = \frac{A_{\lambda 1} - \varepsilon_{\lambda 1}^{RuS} \times l \times [RuCl]}{\varepsilon_{\lambda 1}^{RuOH_2} \times l} \quad (\text{Equation A3})$$

The concentration [RuOH<sub>2</sub>] in Equation 2 can then be substituted with Equation A3, which can then be rewritten as an expression of [RuCl]:

$$[RuCl] = \frac{\varepsilon_{\lambda 1}^{RuOH_2} \times A_{\lambda 2} - \varepsilon_{\lambda 2}^{RuOH_2} \times A_{\lambda 1}}{\varepsilon_{\lambda 1}^{RuOH_2} \times \varepsilon_{\lambda 2}^{RuCl} \times l - \varepsilon_{\lambda 2}^{RuOH_2} \times \varepsilon_{\lambda 1}^{RuCl} \times l} \quad (\text{Equation A4})$$

As the UV-vis samples were not irradiated near the isosbestic points of the photosubstitution reactions, the absorbance at the irradiation wavelength was not constant during the whole irradiation experiment. Thus a procedure that took this fact into account was used to calculate the photochemical quantum yield. The average absorption at the irradiation wavelength  $A_{e,ave}$  between two consecutive UV-vis measurements at  $A_{e,n}$  and  $A_{e,n+1}$  was calculated using Equation A5.

$$A_{e,ave} = \frac{A_{e,n} + A_{e,n+1}}{2} \quad (\text{Equation A5})$$

The amount of moles of photons  $Q_n$  absorbed between two consecutive UV-vis measurements at time  $t_i$  and  $t_{i+1}$ , was calculated according to Equation A6, where  $\Phi$  is the photon flux, the average probability of absorption is given by  $(1 - 10^{-3 \times A_{e,ave}})$ , the factor 3 comes from the 3 cm optical pathlength for irradiation, and  $\Delta t = t_{i+1} - t_i$  is the time between two measurements.

$$Q_n = \Phi \times (1 - 10^{-3 \times A_{e,ave}}) \times \left( \frac{A_{RuCl}}{A_{e,ave}} \right)_n \times \Delta t \quad (\text{Equation A6})$$

Between two consecutive measurements, the fraction of absorbed photons at the excitation wavelength  $A_e$  that can be attributed to the ruthenium thioether complex RuS,  $A_{e,RuCl}$ , is given by Equation A7.

$$\left( \frac{A_{e,RuCl}}{A_{e,ave}} \right)_n = \frac{\left( \frac{A_{e,RuCl}}{A_e} \right)_n + \left( \frac{A_{e,RuCl}}{A_e} \right)_{n+1}}{2} \quad (\text{Equation A7})$$

The total number of moles of photons absorbed at  $t_n$  by the ruthenium thioether complex since the start of the irradiation, noted  $Q(t_n)$ , can be calculated according to Equation A8. The quantum yield was obtained from the slope of a plot of the amount of moles ruthenium thioether ( $n_{RuS}$ ) against  $Q(t_n)$ . Figure S14 depicts the described plots.

$$Q(t_n) = \sum_{i=0}^n Q_i \quad (\text{Equation A8})$$

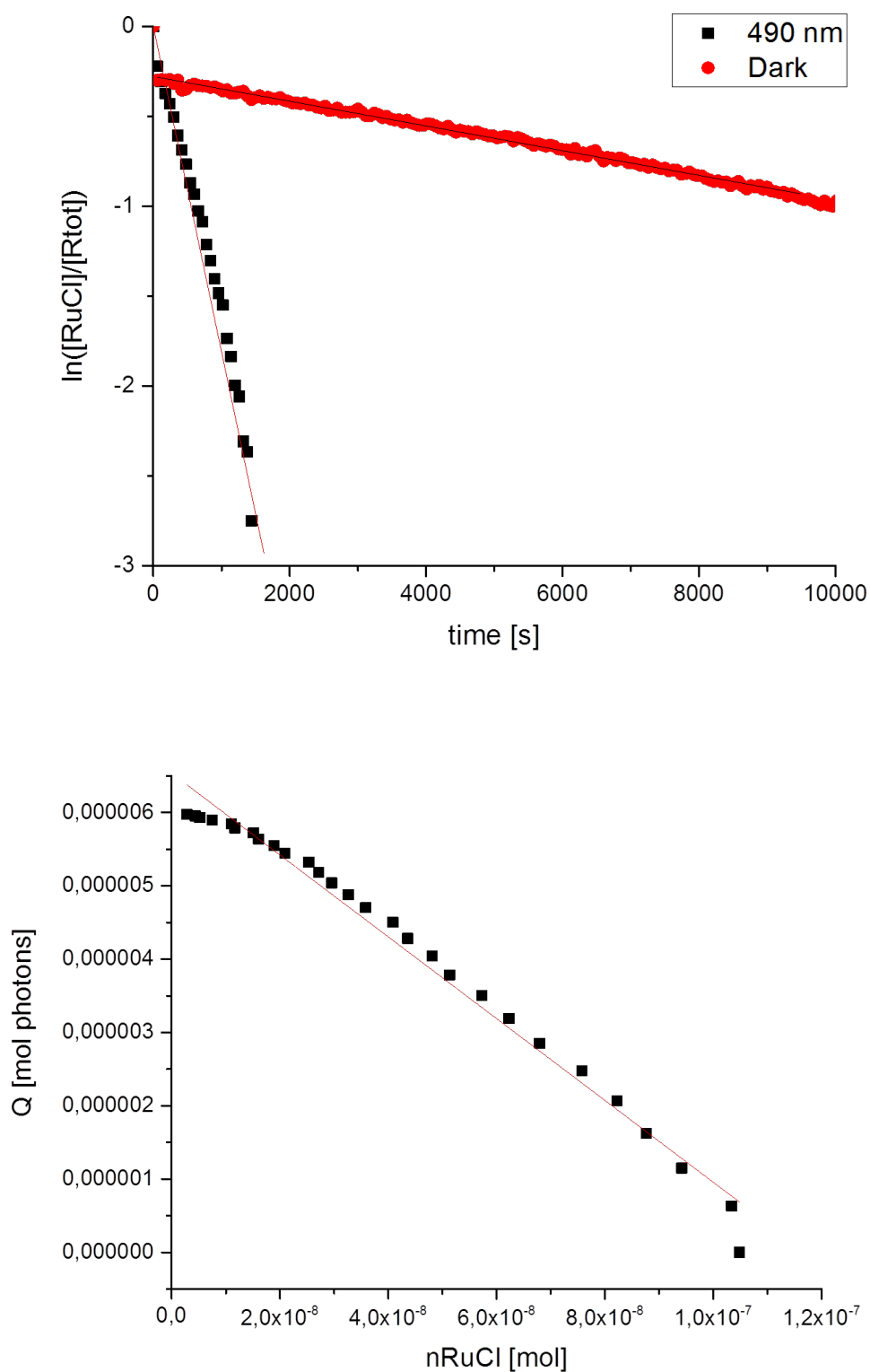


Figure S 14. Above: Plots of  $\ln([\text{RuCl}]/[\text{Ru}_{\text{tot}}])$  vs irradiation time.  $[\text{RuCl}]$  represents the concentration of  $[\mathbf{4}]^+$ , and  $[\text{Ru}]_{\text{tot}}$  the total ruthenium concentration in the solution. The slope of each plot is  $-k_{\phi}$  ( $\text{s}^{-1}$ ). Bottom: Plots of the number of moles of RuCl vs. the number of moles of photons absorbed by RuCl at time  $t$ , since  $t = 0$ ; the slope equals the photosubstitution quantum yield  $\phi$ . Photon fluxes:  $\Phi_{490} = 1.4(4) \times 10^{-8}$  Einstein  $\text{s}^{-1}$

### 3. Self-Assembly of [4]<sup>+</sup>

#### 3.1. Calculation of the Molecular Packing Parameter

##### 3.1.1. General Formula

The molecular packing parameter  $P$  (1), as described by Israelchvili *et al.*<sup>[9]</sup> can be used to predict the morphology of self-assembled surfactants. These estimations are based on the volume ( $v$  in Å<sup>3</sup>), length ( $l$  in Å), and the head group area ( $a_0$  in Å<sup>2</sup>) of the amphiphilic monomer.<sup>[10]</sup>

The values for  $v$  and  $l$  are calculated employing the Tanford equations<sup>[11]</sup>, as described in (2) and (3), with  $n_c$  is the number of carbon atoms of the tail, i.e. 12 for [4]<sup>+</sup>.

$$P = v / (la_0) \quad (1)$$

$$v = 27.4 + 26.9 n_c \quad (2)$$

$$l = 1.5 + 1.265 n_c \quad (3)$$

##### 3.1.2. Deriving Molecule Specific Values for [4]<sup>+</sup>

As depicted in Figure S 15 the head group area  $a_0$  was calculated from the diameters  $d$  obtained from the crystal structure. The calculated value, i.e. 1.04 nm<sup>2</sup> (=103.9 Å<sup>2</sup>) fits well to literature values (~ 1 nm<sup>2</sup>)<sup>[12]</sup> of similar head groups.

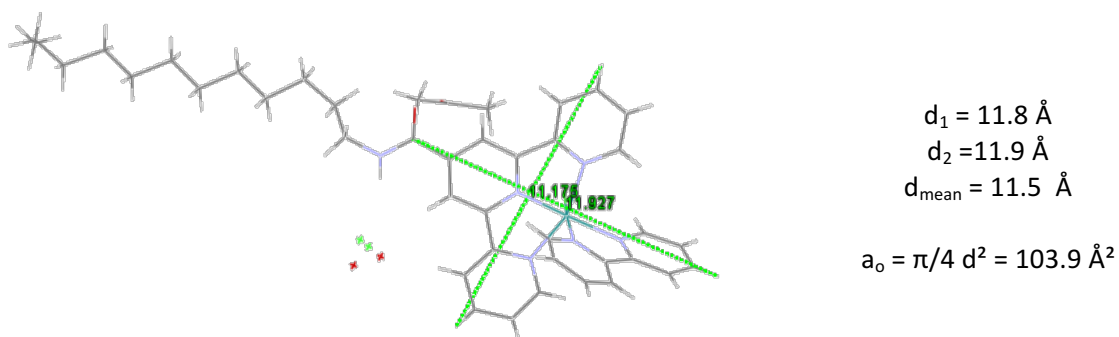


Figure S 15.: Left. Crystal structure of [4]<sup>+</sup> with measured diameters of the head group. Right: Calculation of the head group area  $a_0$ .

##### 3.1.3. Calculation of P

$$P = (27.4 + 26.9 \cdot 12) \cdot (1.5 + 1.265 \cdot 12)^{-1} \cdot (103.9 \text{ \AA}^2)^{-1} = \underline{\underline{0.2}}$$

### 3.2. Dynamic light scattering (DLS) and zeta-potential measurements

Measurements were performed on a Malvern Zetasizer Nano S using disposable plastic cuvettes with 10 mm path length (the measurement angle was set to 173° and a wavelength of 632 nm). Samples were prepared from a stock solution of [4]<sup>+</sup> in DMSO (23.6 mM) and Milli-Q water or PBS buffer to reach a final concentration of 200 μM. Scattered light intensities were monitored for 15 hours to track the evolution of the aggregates. The results are summarized in Table S 5, a representative intensity plot of the size distribution of [4]<sup>+</sup> micelles is shown in Figure S 16. The PBS buffer was diluted in order to reduce the salt concentration to enable ζ-potential measurement. The final salt concentration was 13.7 mM of NaCl. The results are depicted in Table S 5.

Table S 5: Measured particle sizes and zeta-potential values of [4]Cl in MilliQ water or PBS buffer at different time points (1 h and 15 h); hydrodynamic particle diameters (several populations in the sample), and ζ-potential.

Sample (solvent)	Peak 1 (nm)	Peak 2 (nm)	Peak 3 (nm)	ζ-potential (mV)
MilliQ (1 h)	1	45	3824	26.1 ± 7.3
MilliQ (15 h)	-	46	-	28.3 ± 8.4
PBS (1 h)	9	76	5397	19.0 ± 11.1
PBS (15 h)	10	111	4548	23.8 ± 6.8

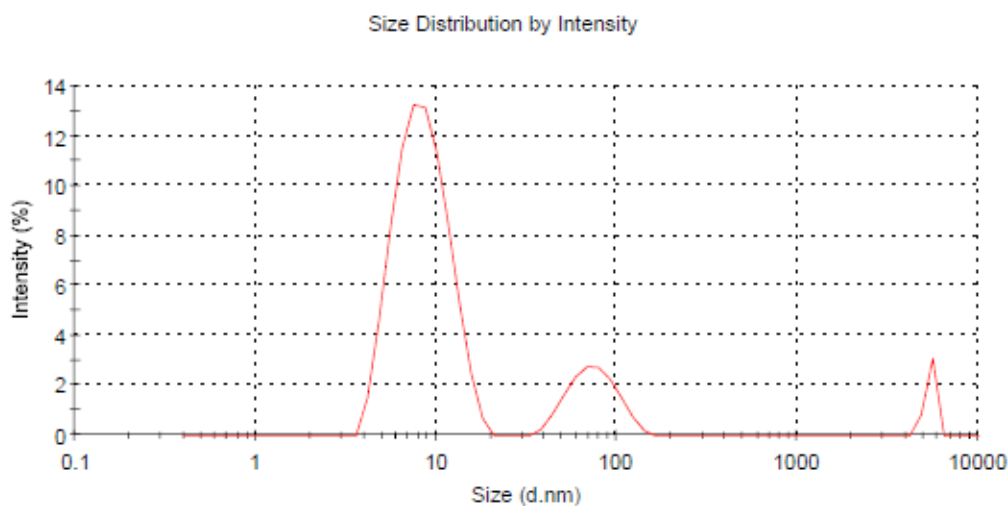


Figure S 16: Size distribution plot of the aggregate structures formed by [4]Cl (200 μM in PBS one hour after preparation)

## 3.2 Cryo-Transmission electron microscopy (cryo-TEM)

Cryogenic TEM samples of [4]Cl in aqueous media were prepared as described above in section 3.1. 5  $\mu\text{L}$  of a colored solution of [4]Cl was pipetted on to a freshly glow-discharged Lacey Carbon Film (300 mesh Cu grids), blotting for 2 seconds and plunge-freezing in liquid ethane at  $-183^\circ\text{C}$  using a Leica EM GP (95% humidity, RT, Whatman No.4 blotting paper). The grids were imaged with a Tecnai F20 equipped with a field emission gun (FEI company) at 200 keV using a Gatan UltraScan camera (Gatan company) with a defocus between  $-3$  and  $-6 \mu\text{m}$  and is depicted in Figure S 17.

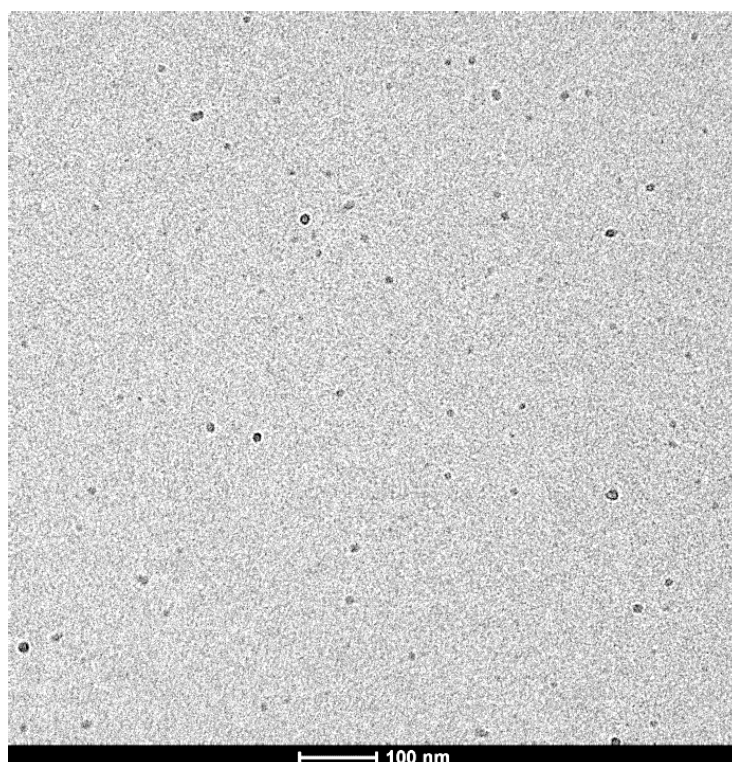


Figure S 17: Cryo-TEM images of [4]Cl in MilliQ water showing micellar aggregates in solution ( $200 \mu\text{M}$ ). Samples were frozen 15 hours after preparation.

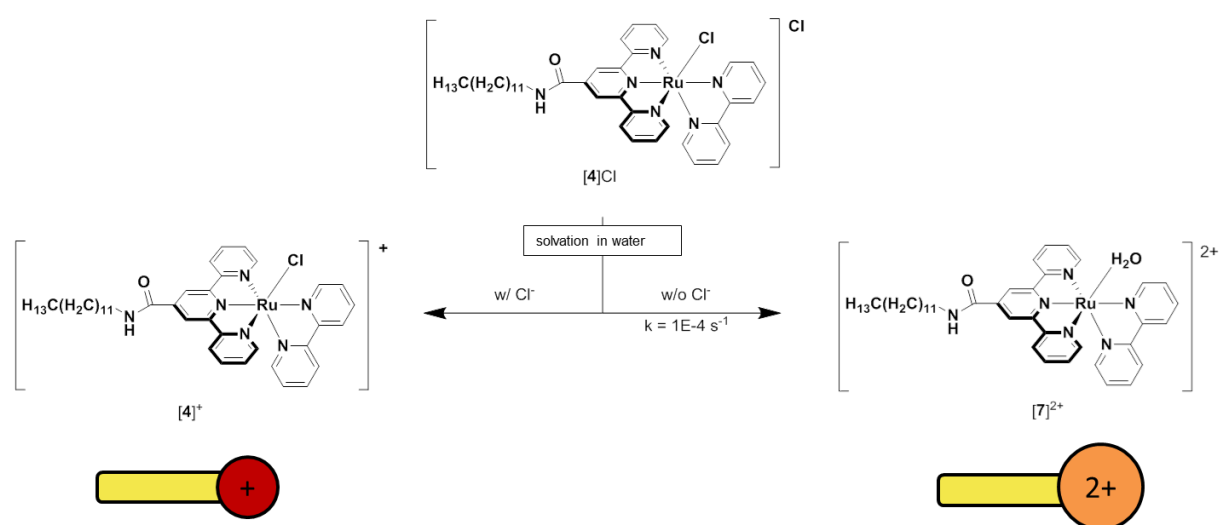


Figure S 18: Solvation of [4]Cl in aqueous solutions. The complex stays stable (for 17 h) in PBS (137 mM NaCl), but hydrolyses to the two-fold positive charged species [7]<sup>2+</sup> in the absence of chloride ions (i.e., when dissolved in MilliQ water). The monomers are schematically depicted, highlighting the difference in charge.

## 4. Biological Studies

### 4.1. Cell Culturing

Cells were thawed and at least passaged twice before starting cytotoxicity experiments. Cells of the cell line A549 were cultured in Dulbecco's Modified Eagle Medium with phenol red, supplemented with 8.0% v/v fetal calf serum (FCS), 0.2% v/v penicillin/streptomycin (P/S), and 0.9% v/v Glutamine-S (GM). Cells were cultured in either 25 cm<sup>2</sup> or 75 cm<sup>2</sup> flasks, and split at 70-80% confluence (three times per week for 25 cm<sup>2</sup> flasks, once per week for 75 cm<sup>2</sup> flasks). The flasks were incubated at 37 °C at 7.0% CO<sub>2</sub>. The medium was refreshed three times a week. Cells used in all biological experiments were cultured for a maximum of 8 weeks. Cells were distributed by the European Collection of Cell Cultures (ECACC), and purchased through Sigma Aldrich. Dulbecco's Minimal Essential Medium (DMEM, with and without phenol red, without glutamine), and 200 mM Glutamine-S (GM) were purchased from Sigma Aldrich. Fetal calf serum (FCS) was purchased from Hyclone. Penicillin and streptomycin were purchased from Duchefa, and were diluted to a 100 mg/mL penicillin/streptomycin solution (P/S). Trypsin and Opti-MEM<sup>®</sup> (without phenol red) were purchased from Gibco<sup>®</sup> Life Technologies. Trypan blue (0.4% in 0.81% sodium chloride and 0.06% potassium phosphate dibasic solution) was purchased from BioRad. Plastic disposable flasks and 96-well plates were from Sarstedt. Cells were counted using a BioRad TC10 automated cell counter with BioRad Cell Counting Slides. Eight well  $\mu$ -slides for confocal microscopy were purchased from Ibidi<sup>®</sup>.

### 4.2. Cytotoxicity Studies

The cytotoxicity of [4]Cl was evaluated using the Sulforhodamine B (SRB)<sup>[13]</sup> microculture colorimetric assay. In short, exponentially growing cells were seeded in Opti-MEM<sup>®</sup> (without phenol red, w/ 2.5% FCS, P/S, and GM) into 96-well plates at  $t = 0$  at the appropriate cell densities (A549 = 5000 cells/well) to prevent confluence of the cells during the experiment. At  $t = 24$  h, the cells were treated with serial dilutions of [4]Cl in Opti-MEM for 1 h, 6 h, 12 h or 24 h. The concentration series depended on the incubation time and was 0.5, 2.5, 5.0, 10.0, 25.0, and 50.0  $\mu$ M for 1 h of incubation, or 0.1, 0.3, 0.6, 1.3, 3.1, and 6.3  $\mu$ M for 6, 12, and 24 h of incubation. The final DMSO concentration per well never exceeded 1.00%, which was proved to be non-toxic for the cells. After 1, 6, 12, or 24 h incubation with the drug-loaded media the media was aspirated and replaced by fresh, warm (37 °C) media.

The percentages of surviving cells relative to compound-free wells were determined 72 h after the beginning of drug exposure, i.e. at  $t = 96$  h, using the SRB assay.<sup>[13]</sup> Briefly, cells were fixed using cold trichloroacetic acid (TCA, 10% w/v) and maintained at 4 °C for 4-48 h. Once fixed, TCA was removed from the wells, plates were gently washed five times with water, stained using 100  $\mu$ L sulforhodamine B (0.6% w/v SRB in 1% v/v acetic acid) for 30-45 minutes, washed with approximately 300  $\mu$ L acetic acid (1% v/v) five times, air dried, and the dye was then solubilized using 10 mM tris base. The absorbance at 510 nm was read using a M1000 Tecan Reader. The SRB absorbance data were used to evaluate the viable cell population in Excel and GraphPad Prism. The absorbance data from three wells (technical replicates,  $n_t = 3$ ) for each cell line and concentration, were averaged. Relative cell populations were calculated by dividing the average absorbance of the irradiated wells by the average absorbance of the dark control. Three biological replicates ( $n_b = 3$ ) of each treatment and cell line were completed, if not otherwise stated. The averages of the biological replications were plotted as relative cell population vs. log(concentration in  $\mu$ M) with standard error of each

concentration. For each cell line the EC<sub>50</sub> was calculated by fitting the logarithmic dose-response curves using non-linear regression with fixed Y maximum (100%) and minimum (0%) relative cell population, and a variable Hill-slope, resulting in the simplified two parameter Hill-slope equation using PRISM 5.0.

Table S6: Cell growing inhibition effective concentration (EC<sub>50</sub> values with 95% confidence interval in μM) for complex [4]Cl in A549 cancer cells. Values were obtained as described in 4.2. \*obtained as biological duplicate.

Incubation time	[4]Cl	95% confidence Interval (in μM)		[3]Cl
		(+)	(-)	
1 h	9.8	1.7	1.5	> 100
6 h	5.6	1.2	1.0	> 100
12 h	4.4	0.7	0.6	> 100
24 h	2.2*	2.2*	0.3	> 100

### 4.3. Microscopic Uptake Studies

Cells were seeded in eight well chamber slides at a concentration of 25000 cells/ml in OMEM (2.5% FCS) and allowed to grow for 24 h. After refreshing the media, the slide were mounted under the microscope, and 0.5 μL of a 4 mM stock solution of [4]Cl in DMSO was added while the microscope was recording. For longer incubation studies the compound was added after refreshing the media, and the slide was returned to the incubator (37 °C, 7% CO<sub>2</sub>) for the duration of incubation. The cells were excited at 488 nm, and the emission was collected between 650-850 nm. Averages of six pictures were acquired. Time-lapse studies were done using green light excitation (532 nm), to avoid cell toxicity effects upon prolonged blue light irradiation of the cells. Control cells didn't show any auto fluorescence with the chosen settings. Pictures were processed with ImageJ, to express the luminescence intensity along across the cells. [Video-1](#) represents a time-laps of the first twenty minutes of uptake. The compound was added after the first picture (control) was taken. [Video-2](#) represents a z-stack throughout the cell, underlining absence of the complex in the nuclei.

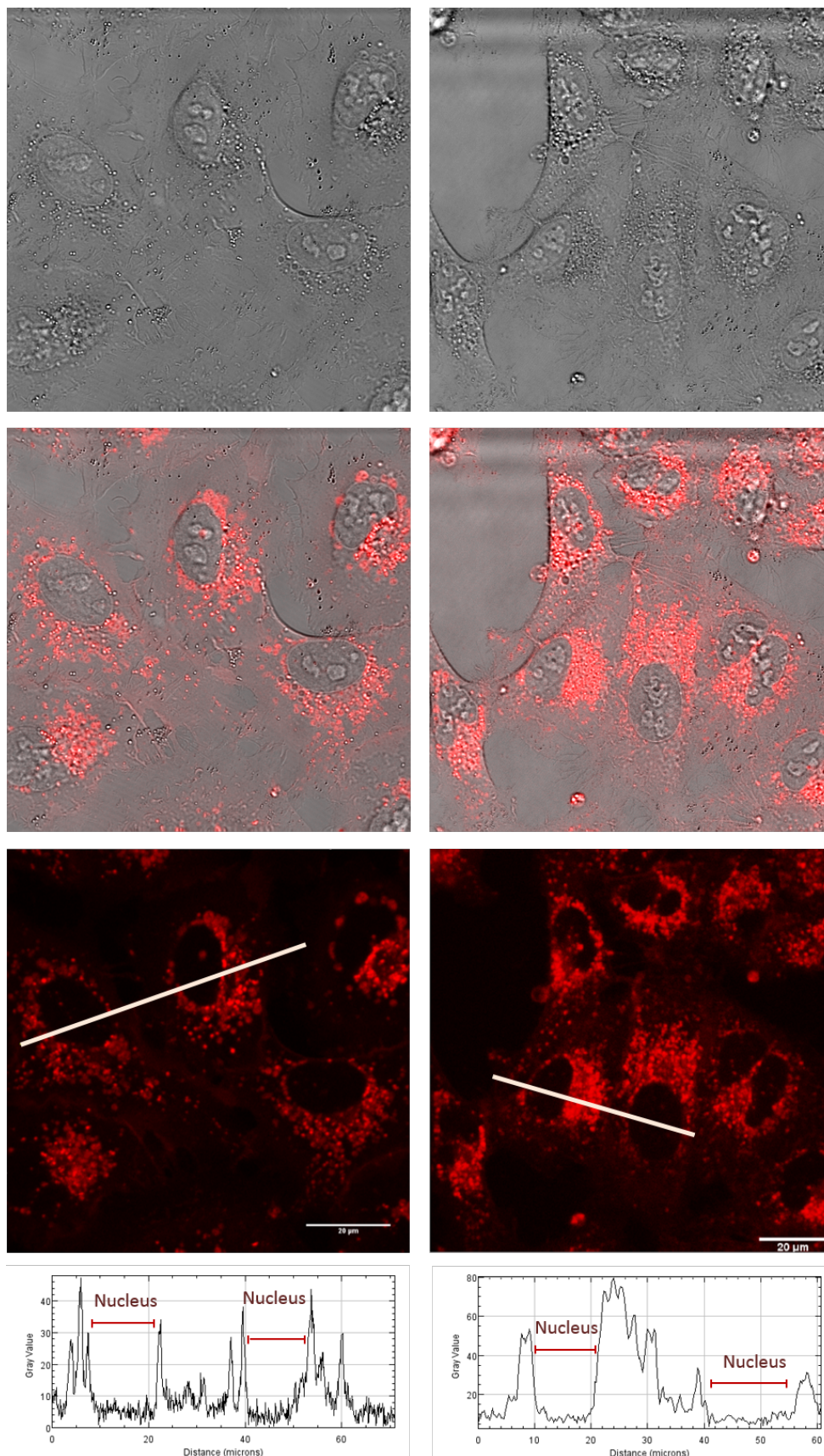


Figure S19: Confocal microscopy images (63x magnification) of A549 cells treated with  $[4]Cl$  ( $5 \mu M$ ) for 9 h (left column) or 22 h (right column). From the top to the bottom are given bright field, merged, red emission (phosphorescence of  $[4]^+$ ), and an emission intensity plot along the white lines. The latter shows clearly that there is no significant emission inside the nucleus.

## 5. DFT calculations

[4]<sup>+</sup> was minimized by DFT in the vacuum using the BPE0 functional and TZP as a basis set, as implemented in the ADF program from SCM. The crystal structure was used as starting geometry. The HOMO and LUMO orbital of the converged geometry are shown in Figure S20.

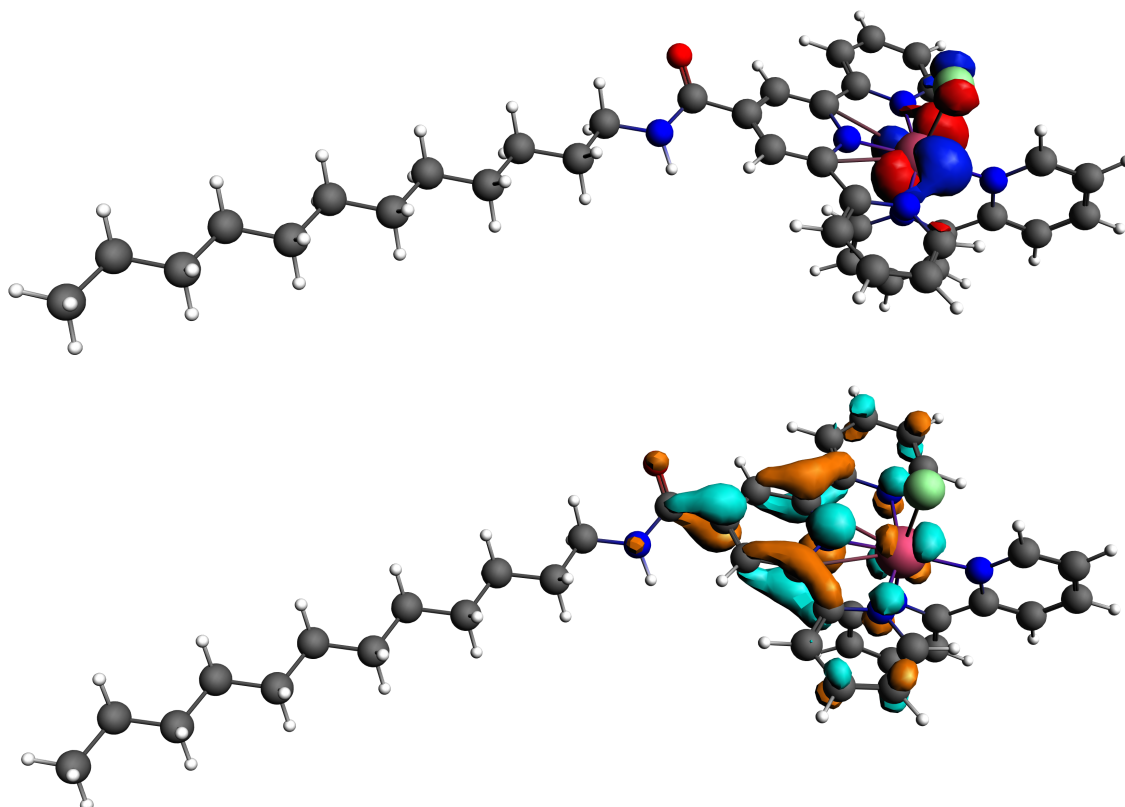


Figure S20. HOMO (top) and LUMO (bottom) orbital of [4]<sup>+</sup> minimized by DFT in vacuum at the DFT/PBE0/TZP level.

## 6. Literature

- [1] A. Bahreman, B. Limburg, M. A. Siegler, E. Bouwman, S. Bonnet, *Inorg. Chem.* **2013**, *52*, 9456-9469.
- [2] G. M. Sheldrick, *Acta crystallographica. Section C, Structural chemistry* **2015**, *71*, 3-8.
- [3] S. H. C. Askes, A. Bahreman, S. Bonnet, *Angewandte Chemie International Edition* **2014**, *53*, 1029-1033.
- [4] J. Ravensbergen, F. F. Abdi, J. H. van Santen, R. N. Frese, B. Dam, R. van de Krol, J. T. M. Kennis, *The Journal of Physical Chemistry C* **2014**, *118*, 27793-27800.
- [5] J. J. Snellenburg, S. P. Laptanok, R. Seger, K. M. Mullen, I. H. M. van Stokkum, *J Stat Softw* **2012**, *49*, 1-22.
- [6] I. H. M. van Stokkum, D. S. Larsen, R. van Grondelle, *Bba-Bioenergetics* **2004**, *1657*, 82-104.
- [7] J. T. M. Kennis, M. L. Groot, *Curr Opin Struc Biol* **2007**, *17*, 623-630.
- [8] K. C. Toh, E. A. Stojkovic, I. H. van Stokkum, K. Moffat, J. T. Kennis, *Physical chemistry chemical physics : PCCP* **2011**, *13*, 11985-11997.

- [9] J. N. Israelachvili, D. J. Mitchell, B. W. Ninham, *J. Chem. Soc., Faraday Trans.* **1976**, *72*, 1525-1568.
- [10] R. Nagarajan, *Langmuir* **2002**, *18*, 31-38.
- [11] C. Tanford, *J Phys Chem* **1972**, *76*, 3020-3024.
- [12] P. C. Griffiths, I. A. Fallis, T. Tatchell, L. Bushby, A. Beeby, *Adv. Colloid Interface Sci.* **2008**, *144*, 13-23.
- [13] V. Vichai, K. Kirtikara, *Nat Protoc* **2006**, *1*, 1112-1116.